Jordanian Journal of Computers and Information Technology (JJCIT), Vol. 04, No. 02, August 2018.

PATH LOSS ESTIMATION FOR BONE IMPLANTABLE APPLICATIONS

Rula Alrawashdeh

(Received: 5-Jan.-2018, Revised: 24-Mar.-2018, Accepted: 9-Apr.-2018)

ABSTRACT

The implantable body sensor network (IBSN) has many promising applications. The sensors in the network support different functionalities, such as glucose monitoring and strain measurement in bones. These sensors work with a central hub that communicates with a receiver outside the body. A reliable communication link between these sensors is essential. In this paper, the path loss between elliptic circular loop antennas in muscle and two different bones (the humerus and femoral bone) has been estimated at 403 MHz inside the CST Katja voxel body model. A 33 dB larger path loss is obtained between muscle and humerus antennas than that between muscle and femoral bone antennas. Hence, a standard link with an ideal phase shift keying (PSK) can be only built up from the femoral bone to the the muscle above the hip. The results in this paper provide a good source of data for link budget calculations for bone implantable applications.

KEYWORDS

EIRP, IBSN, ISM, MedRadio, PSK.

1. INTRODUCTION

Implantable devices have many important applications in healthcare and biomedical telemetry [1]-[2]. An antenna is normally used with the implantable device to transfer the biological data wirelessly from this device to a receiver [3]-[4]. The receiver is placed at different positions (in the human body, on or outside of it) to suit different applications. Hence, different communication links (in-in, in-on and in-off body) can be established [5]-[11]. These links should be characterized and their losses should be carefully estimated. The path loss between implantable and off-body antennas was estimated in [9]. It was also estimated between implantable and on-body antennas in [6]-[7]. In implantable body sensor network (IBSN), different implantable sensors can exist and work with each other. For example, a glucose monitoring implant can work with a pacemaker/central hub, which then can communicate with a receiver placed outside the human body. This is very beneficial, as the communication from inside the human body to an external receiver needs to take place from one implant only [5], [12]. However, the path loss should be evaluated in anatomical body models considering actual and exact positions of implantations, in order to obtain accurate results. The path loss between different muscle implants was estimated in [12]-[13] using flexible dipole antennas at 2.45 GHz. In [14], the path loss was experimentally measured within 2.36-2.5 GHz in a homogeneous liquid body phantom of small dimensions ($30\times 30\times 20$ cm^3). However, the losses in that paper were measured for paths in a simplified body phantom that did not provide a good resemblance of the real human body. In [11], a communication link between a transmitting half-wave dipole in the pancreas tissue and a probe receiver placed in different points in the human mesh was characterized at 2.45 GHz and its path loss was modeled. The 401-406 MHz Medical Device Radiocommmunication Service (MedRadio) band is mainly allocated for implantable applications. The attenuation in the human body tissues within the MedRadio band is smaller than that within the 2.45 GHz Industrial Scientific and Medical (ISM) band. The path loss in this band was estimated in [5] and [11] at 402.5 and 403 MHz, respectively. However, none of these paths was in bones or between bone and muscle implantable antennas. Bone implants have many important applications, such as bone healing, growth and checkups of artificial joints [15]-[16]. Different antenna designs were proposed for bone implants [17]-[21]. Bone implants may exist with other muscle implants in the IBSN. Therefore, it is very beneficial to quantify the losses of communication paths between bone and muscle implants for different applications.

Rula Alrawashdeh is with Department of Electrical Engineering, Mutah University, Alkarak, Jordan. Email: rularsr18@gmail.com

In this paper, the path loss between bone and muscle implantable loop antennas has been estimated and quantified at 403 MHz inside simplified and anatomical Katja voxel body models. The implantable antennas are first designed in simplified body models to accelerate the overall design process. Then, they are simulated in the anatomical body model to obtain accurate results about the path losses. The bone implantable antenna is placed inside the humerus or femoral bone, while the muscle implantable antenna is placed in the muscle above the left hip.

This paper is organized as follows: First, the design of both antennas in the simplified body model is presented. Then, performance of antennas is evaluated and validated in the CST Katja voxel body model. After that, the losses of the communication paths between muscle and bone antennas are estimated and the link budgets are calculated. Finally, the paper is concluded.

2. SETUP AND CONFIGURATION

Flexible elliptic circular loop antennas are used for the analysis in this paper. This is because loop antennas are more efficient in the lossy human body than electrical type antennas [22]-[24]. The antenna is bent around cylindrical implants of the following dimensions:

5 mm in radius and 11 mm in length for the glucose monitoring implant in the muscle above the left hip.
8 mm in radius and 56 mm in length for the implant in the humerus and femoral bone.

Both antennas have the same shape as shown in Figure 1. However, they have different dimensions as summarized in Table 1.

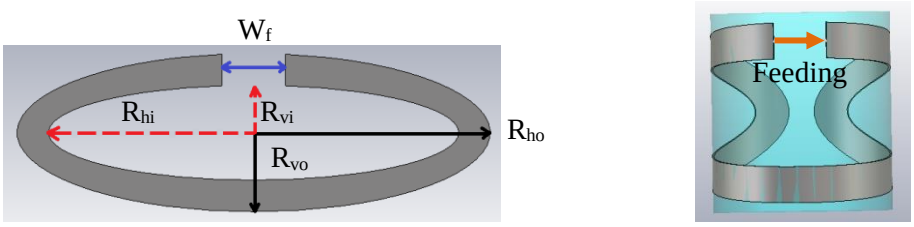

(a) (b)

Figure 1. The proposed antennas structure: (a) flat, (b) bent views.

Table 1. The dimensions of the proposed antennas.

Parameter	**Symbol**	**Dimensions (mm)**	
		Muscle implantable antenna	**Bone implantable antenna**
The outer horizontal radius	R_{ho}	15	28
The inner horizontal radius	R_{hi}	13	23
The outer vertical radius	R_{vo}	5	18
The inner vertical radius	R_{vi}	3	17
Feeding gap width	W_f	3	4

Bone implants are usually larger in size than muscle implants [16], [21] and hence the bone implantable antenna is designed with larger physical dimensions.

The human body tissues are lossy and their dielectric properties are frequency dependent. The antennas are simulated in the middle of simplified human body models. These models are conical in shape and have the following properties:

- Of a single homogeneous layer of ($\varepsilon_r = 57.1$ and $\sigma = 0.79\ S/m$ which resembles the dielectric properties of muscle at 403 MHz [25]). The antenna intended for implantation in the muscle above the left hip is designed inside of this body model.
- Of two layers; outer muscle layer of ($\varepsilon_r = 57.1$ and $\sigma = 0.79\ S/m$) and inner bone layer of ($\varepsilon_r = 13.14$ and $\sigma = 0.09\ S/m$), which resemble the dielectric properties of muscle and bone cortical, respectively at 403 MHz [25]. The antenna intended for implantation in the humerus and femoral bone is designed in the middle of the bone layer of this model.

Jordanian Journal of Computers and Information Technology (JJCIT), Vol. 04, No. 02, August 2018.

Top and side views of the simplified human body models are shown in Figure 2.

The simplified body models are much smaller in size than the anatomical body models. They are also of uniform layers, as indicated above. Therefore, the simulation time inside of these models is much shorter than that in the anatomical body models. Hence, the overall design process will be accelerated if the antenna structure is optimized first in the simplified body model and then evaluated in the anatomical body model [5, 22, 26]. The antenna performance may be altered in the anatomical body model, which has a better resemblance of the real human body. However, if the antenna is broad in bandwidth, its matching will be maintained (S11≤ -10 dB) within the band of interest (401-406 MHz MedRadio band for the case of this paper) [5]. Also, the process of optimizing the antenna structure in the simplified body helps in understanding the antenna structure and its effective parameters. Hence, small modifications are only expected to be made in the anatomical body model if needed.

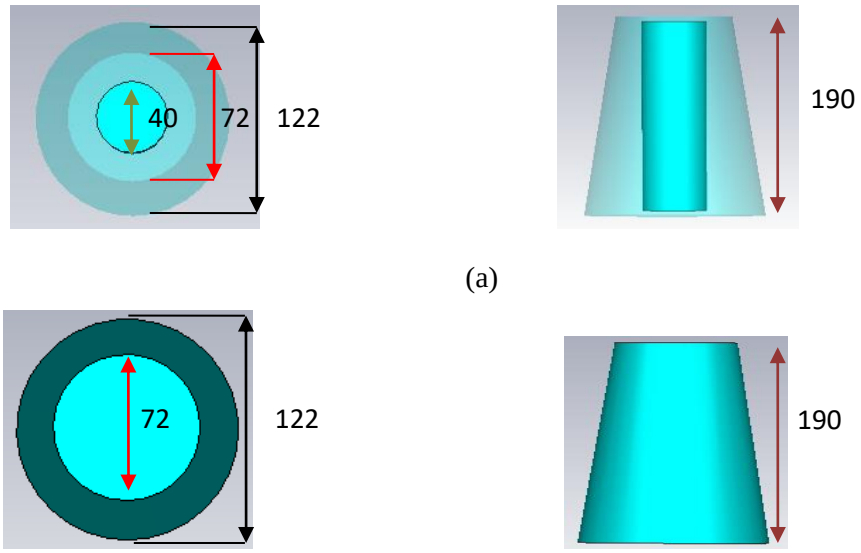

Figure 2. Top and side views of the: (a) two-layer (bone-muscle) and (b) single-muscle layer simplified body model; dimensions in mm.

3. PERFORMANCE

In this section, the simulated reflection coefficient S11 and realized gain of the proposed antennas will be evaluated and discussed in the simplified and CST Katja voxel body models.

3.1 Performance in the Simplified Body Model

The proposed antennas are simulated at the centre of the simplified body models. Simulations are conducted using the CST microwave studio [27]. Hexahedral meshes are employed and a minimum distance of λ/8 is kept between the structure and the edge of the simulation space. The antennas are fed by discrete ports of 50 Ω with an input power of 1 W. The antenna is designed to obtain a broad bandwidth of wider than 200 MHz around 403 MHz. This is to guarantee a robust performance of the antenna if detuning happens in the anatomical and actual human bodies. The simulation results are shown in Figure 3. Both antennas obtain good matching (S11≤ -10 dB) at 403 MHz. The realized gain values for the simulated antennas are -22 and -35.61 dBi for the bone and muscle implantable antennas, respectively at 403 MHz. The bone implantable antenna has obtained a larger gain than that for the muscle implantable antenna. This is because the bone implant is larger in size than the muscle implant. Hence, the lossy area surrounding it will be smaller than that surrounding the muscle implant. Moreover, the bone has a smaller conductivity than that for muscle ($\sigma = 0.09$ and 0.79 S/m for bone cortical and muscle, respectively [25]). This reduces the near field coupling between the antenna and the surrounding human body tissue which reduces the power loss due to absorption. Hence, a larger gain is obtained. The muscle implantable antenna has obtained a good matching (S11≤-10 dB) as desired. Although the antenna bandwidth is not centered at 403 MHz, a good matching is expected to be maintained in the anatomical body model. This

is because the antenna is intended for implantation in the area above the left hip in close proximity to some organs of the digestive tract, such as the small intestine. The relative permittivity of these organs is larger than that for muscle (57.1 for muscle and 66 for the small intestine at 403 MHz [25]) and hence the resonant frequency is expected to be the same or shifted down, but not shifted up in the anatomical body model. It will be shown in a following section that S11 is also smaller than -10 dB at 403 MHz in the anatomical body model, as expected.

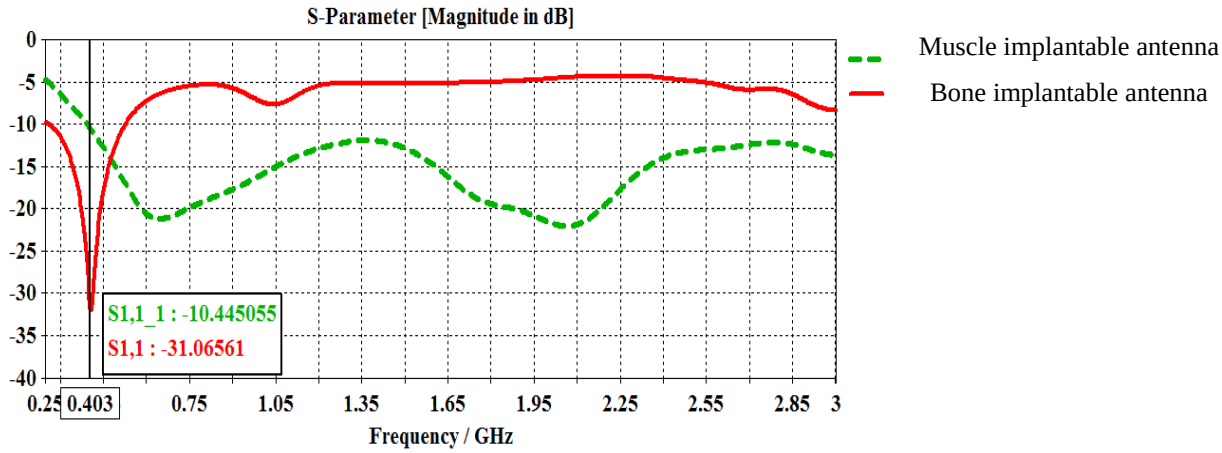

Figure 3. The reflection coefficient S11 (dB) for the muscle and bone implantable antennas in the simplified body models.

3.2 Performance in the Anatomical Body Model

In order to estimate the path loss accurately, it is very important to simulate the antennas at the exact positions of implantations inside the anatomical body model. The anatomical body model is composed of non-uniform and heterogeneous tissues that resemble the real human body tissues [28]. These models are provided by different simulation tools, such as CST. The CST Katja voxel body model is used for the simulations in this paper. The CST Katja voxel body model represents a 43-year old female with height of 163 cm and weight of 62 kg [29]. The bone implantable antenna in this paper is placed in the humerus or femoral bone, while the muscle implantable antenna is placed in the muscle above the left hip. It is worth indicating that in order to provide accurate comparison, the same antenna is simulated in the humerus and femoral bone. The positions of implantation in the anatomical body model are shown in Figures 4 and 5. The muscle implantable antenna is placed in the muscle above the left hip, directly beneath the fat layer. Bone implantable antennas are placed at the centre of the humerus and femoral bones. All antennas are oriented to the front such as in Figure 1 (b).

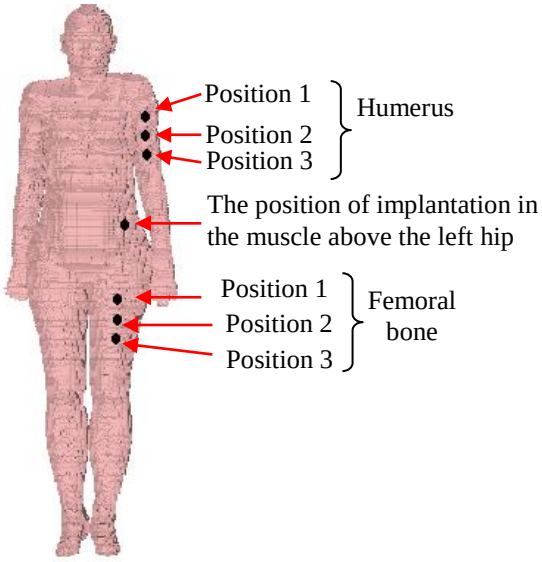

Figure 4. Positions of implantation in the CST Katja voxel body model (front view of the human body).

Jordanian Journal of Computers and Information Technology (JJCIT), Vol. 04, No. 02, August 2018.

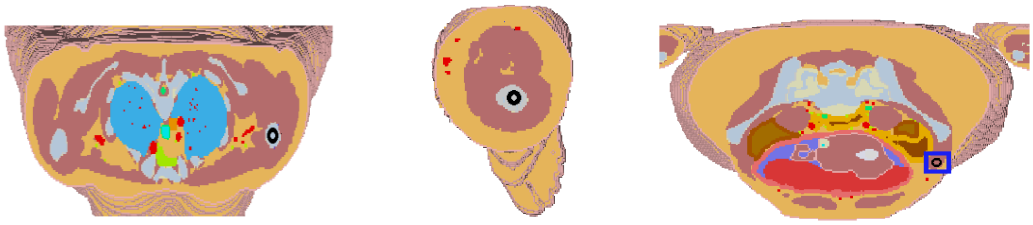

Figure 5. Positions of implantation (indicated by the black ring) in the CST Katja voxel body model (top view).

Two links are first simulated at 403 MHz. One between the implantable antenna in the humerus at position 1, which is 15 mm above the armpit, and the antenna in the muscle above the left hip. The other one is established between the antenna in the femoral bone at position 1, which is at 20 mm from the top of the femoral bone, and the antenna in the muscle above the left hip. The antenna in the muscle above the left hip is simulated at a fixed position which is shown in the figure. This position is popular for glucose monitoring implants [5], [21]. The results of the simulated reflection coefficient are shown in Figure 6.

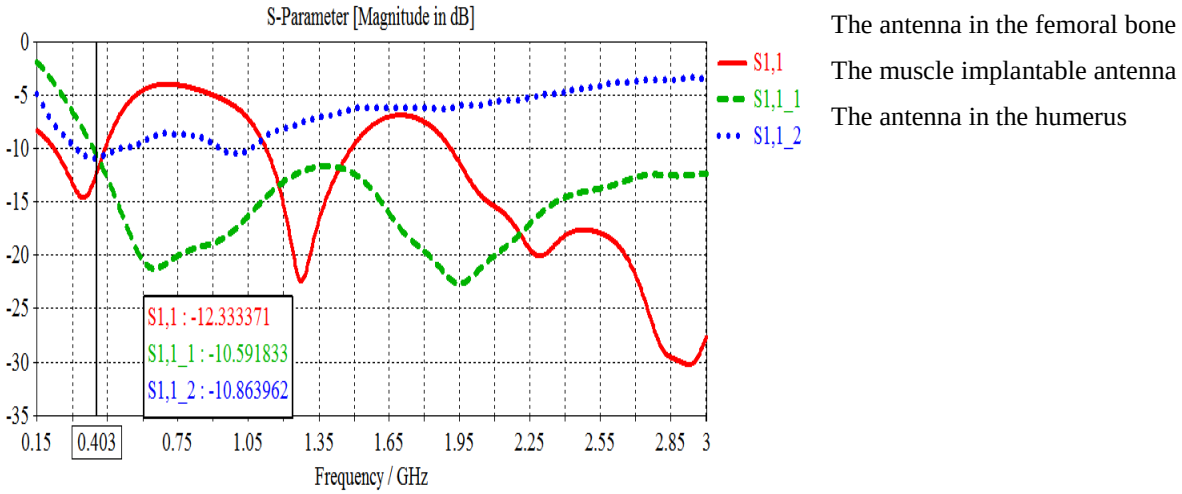

Figure 6. The reflection coefficient S11 (dB) for the muscle and bone implantable antennas at position 1 in the CST Katja voxel body model.

The results in the figure show that a good matching (S11≤ -10 dB) is obtained at 403 MHz for all of the three cases of implantation in the muscle and both bones. To provide more options for actual implantation in the human body, two other positions of implantation in the humerus and femoral bones are attempted (positions 2 and 3 shown in Figure 4). A distance of 10 mm is kept between the two positions. The simulated reflection coefficient obtained a good matching (S11≤ -10 dB) for all of these positions.

4. Path Loss Estimation and Link Budget Calculations

This section aims at estimating the losses of both of the communication links indicated above and calculating the corresponding link budget.

4.1 Simulated Path Losses and Link Parameters

The path loss (P_L) is defined as the inverse of the transmission coefficient (S_{21}) between the transmitting and receiving implantable antennas, which are matched to 50 Ohms (1) [12].

$$P_L\left(dB\right)=\left(\frac{P_{in}}{P_{Rx}}\right)=-10\log_{10}\left|S_{21}\right|^2=-\left|S_{21}\right|\left(dB\right) \quad (1)$$

where P_{in} (W) is the power input to the transmitting antenna and P_{Rx} (W) is the power received at the receiving antenna.

The simulated path losses between the transmitting and receiving antennas investigated in this paper are summarized in the Table 2.

Table 2. The muscle-humerus and muscle-femoral bone path loss P_L (dB) at the three positions of implantation.

	Position 1	**Position 2**	**Position 3**
Muscle - humerus	123 dB	121.4	120
Muscle - femoral bone	86.15	87.8	90

The largest path loss is obtained at position 1 and position 3 at the humerus and femoral bone, respectively. The distance between the muscle and bone implantable antennas at these positions is the largest amongst all cases of the three positions of investigation. When the distance increases, the path loss increases accordingly.

A link of the parameters summarized in Table 3 is considered. This link was considered in [12] to evaluate the communication path links between muscle implantable devices. The links investigated in this paper will be also evaluated based on the parameters of this link.

Table 3. Parameters of a communication link between muscle and bone implantable devices.

Link parameter	**Value**
Transmitted power, P_{TX} (μW)	25
Ambient temperature, AT (K)	310
Bit rate, B_r (Kb/s)	7
Boltzmann's constant, K_B (J/K)	1.38×10^{-23}
Coding gain, G_c (dB)	0
Fixing or deterioration gain, G_d (dB)	2.5
Energy per bit to noise power spectral density ratio, E_b/N_0 (dB) (ideal PSK)	9.6
Noise spectral density, N_0 (dBm/Hz)	-173
Bit error rate (BER)	1×10^{-5}

The power is limited to up to 25 μW in the 401-406 MHz MedRadio band [30] to prevent hazardous heating of the biological tissues. Phase Shift Keying (PSK) modulation is assumed. In terms of bit error rate (BER), PSK exhibits considerable advantage over Frequency Shift Keying (FSK) and Amplitude Shift Keying (ASK) at the same amplitude levels [31]. The coding is assumed to present no gain to the system for worst-case consideration.

4.2 Link Budget Calculations

The communication is build up when the link carrier to noise density $(\frac{C}{N_0})$ exceeds the required $(\frac{C}{N_0})$ referring to Eqs. (2 and 3) [12]:

$$\text{Link}\left(\frac{C}{N_0}\right)(dB) = P_{TX}\,(dB) - P_{L,organ}\,(dB) - N_0(dB) \quad (2)$$

$$\text{Required}\left(\frac{C}{N_0}\right)(dB) = \left(\frac{E_b}{N_0}\right)(dB) + 10\,log_{10}(B_r) - G_c(dB) + G_d(dB) \quad (3)$$

Considering the link parameters in Table 3, the required $\left(\frac{C}{N_0}\right)$ is calculated as 50.55 dB. The link $\left(\frac{C}{N_0}\right)$ should be larger than 50.55 dB for this communication to build up. To satisfy this, the path loss should be samller than 106.45 dB. This can be obtained for the communication link between the glucose monitoring implant in the muscle above the left hip and the implant in the femoral bone for all of the investigated locations, but not with that for any location in the humerus.

5. CONCLUSIONS

In this paper, the path loss between a glucose monitoring implant and bone implants in the humerus and

femoral bone has been estimated and quantified. The glucose monitoring implant is simulated in the muscle above the left hip. The path loss increases with distance. Therefore, the path loss of the link from the humerus to the glucose monitoring implant is larger than that from the femoral bone. A loss of up to 123 dB is obtained for the path between the implant in the muscle above the left hip and that in the humerus. A loss of up to 90 dB is obtained between the implant in the muscle above the left hip and that in the femoral bone. Based on the results in this paper, it can be concluded that a glucose monitoring implant in the muscle above the left hip can communicate with the implant in the femoral bone, but not with that in the humerus considering the parameters of a typical communication link between implants based on PSK modulation. For future work, different channels between the femoral bone and other implants for different applications will be fully characterized and their path losses will be modelled.

REFERENCES

[1] K. D. Barnard, "Acceptability of Implantable Continuous Glucose Monitoring Sensor," Jou. Diabetes Sci. Technol., vol. 2017, Oct. 2017.

[2] H. Belham et al., "Implantable Strain Sensor to Monitor Fracture Healing with Standard Radiography," Scientific Report, vol. 7, no. 1489, May 2017.

[3] K. Zhang, C. Liu, X. Liu, H. Guo and X. Yang, "Miniaturized Circularly Polarized Implantable Antenna for ISM-Band Biomedical Devices," International Journal of Antennas and Propagation, vol. 2017, pp. 1-9, March 2017.

[4] M. Kod et al., "Feasibility Study of Using the Housing Cases of Implantable Devices as Antennas," IEEE Access, vol. 4, pp. 6939-6949, Sep. 2016.

[5] R. Alrawashdeh, Implantable Antennas for Biomedical Applications, Ph.D. Dissertation, Dept. Elect. Eng., Liverpool Univ., Liverpool, UK, 2015.

[6] P. A. Floor et al., "In-Body to On-Body Ultra-wideband Propagation Model Derived from Measurements in Living Animals," IEEE Jou. of Biomedical and Health Informatics, vol. 19, no. 3, pp. 938-948, May 2015.

[7] A. Stango, K. Y. Yazdandoost, F. Negro and D. Farina, "Characterization of In-Body to On-Body Wireless Radio Frequency Link for Upper Limb Prostheses," PLoS One 11(10): e0164987, Oct. 2016.

[8] A. Alomainy and Y. Hao, "Modeling and Characterization of Biotelemetric Radio Channel from Ingested Implants Considering Organ Contents," IEEE Transactions on Antennas and Propagation, vol. 57, no. 4, pp. 999-1005, April 2009.

[9] D. Kurup, G. Vermeeren, E. Tanghe, W. Joseph and L. Martens, "In-to-Out Body Antenna-Independent Path Loss Model for Multi-layered Tissues and Heterogeneous Medium," Sensors, vol. 15, pp. 408-421, Jan. 2015.

[10] Y. Liao, M. S. Leeson and M. D. Higgins, "A Communication Link Analysis Based on Biological Implant Wireless Body Area Networks," Applied Computational Electromagnetics Society Journal, June 2016.

[11] T. Chrysikos, I. Zisi and S. Kotsopoulos, "Channel Modeling and Path Loss Characterization for In-body Propagation at MICS and ISM Bands," Wireless Telecommunication Symposium (WTS 2016), London, pp. 1-7, 2016.

[12] D. Kurup, W. Joseph, G. Vermeeren and L. Martens, "Specific Absorption Rate and Path Loss in Specific Body Location in Heterogeneous Human Model," IET Microwaves, Antennas & Propagation, vol. 7, no. 1, pp. 35-43, Jan. 2013.

[13] D. Kurup et al., "In-Body Path Loss Models for Implants in Heterogeneous Human Tissues Using Implantable Slot Dipole Conformal Flexible Antennas", EURASIP Journal on Wireless Communications and Networking, vol. 2011, no. 54, pp. 1-9, 2011.

[14] R. Chavez-Santiago et al., Experimental Path Loss Models for In-Body Communications within 2.36–2.5 GHz, IEEE Journal of Biomedical and Health Informatics, vol. 19, no. 3, pp. 930-937, May 2015.

[15] Guide to Knee Replacement Implants and Their Manufacturers, [Online], Available: https://www.healthline.com/health/total-knee-replacement-surgery/implant-manufacturers

[16] J. A. López-López et al., "Choice of Implant Combinations in Total Hip Replacement: Systematic Review and Network Meta-analysis," BMJ, Nov. 2017.

[17] D. Karnaushenko, D. Makarov and O. G. Schmidt, "Compact Helical Antenna for Smart Implant Applications," NPG Asia Mterials 7, June 2015.

[18] R. Alrawashdeh, Y. Huang and P. Cao, "A Flexible Loop Antenna for Total Knee Replacement Implants in the MedRadio Band," Proc. LAPC, Loughborough, UK, pp. 225-228, 2013.

[19] P. Zakavi, N. C. Karmakar and I. Griggs, "Wireless Orthopedic Pin for Bone Healing and Growth: Antenna Development," IEEE Transactions on Antennas and Propagation, vol. 58, no. 12, pp. 4069-4074, Dec. 2010.

[20] S. Symeonidis, W. G. Whittow, C. Panagamuwa and M. Zecca, "An Implanted Antenna System for the Monitoring of the Healing of Bone Fractures," Loughborough Antennas & Propagation Conference (LAPC 2015), Loughborough, pp. 1-4, 2015.

[21] M. K. Magill, G. A. Conway and W. G. Scanlon, "Robust Implantable Antenna for In-body Communications," Loughborough Antennas & Propagation Conference (LAPC 2015), Loughborough, pp. 1-4, 2015.

[22] F. Merli, Implantable Antennas for Biomedical Applications, Ph.D. Dissertation, Dept. Elect. Eng., EPFL Univ., Lausanne, Switzerland, 2011.

[23] R. Alrawashdeh, "A Review on Wireless Power Transfer in Free Space and Conducting Lossy Media," Jordanian Journal of Computers and Information Technology (JJCIT), vol. 3, no. 2, pp. 71-88, Aug. 2017.

[24] Y. El-Saboni, G. A. Conway and W. G. Scanlon, "The Importance of Antenna Near-Field Losses in Intra-Body UHF Communication Applications," IEEE International Symposium on Antennas and Propagation & USNC/URSI National Radio Science Meeting, San Diego, CA, pp. 399-400, 2017.

[25] "Calculation of the Dielectric Properties of Body Tissues," Institute for Applied Physics, Italian National Research Council, [Online], Available: http://niremf.ifac.cnr.it/tissprop/

[26] A. Kiourti and K. S. Nikita, "Methodologies for Fast and Accurate Design of Implantable Antennas: Analysis and Comparison," 7th European Conference on Antennas and Propagation (EuCAP 2013), Gothenburg, pp. 579-582, 2013.

[27] CST - Computer Simulation Technology, [Online], Available: http://www.CST.com

[28] R. Alrawashdeh, Y. Huang and Q. Xu, "Evaluation of Implantable Antennas in Anatomical Body Models," CST-article 2014.

[29] CST Studio Suite, BioEM Simulation Using CST STUDIO SUITE 2013, [Online], Available: https://www.cst.com/Content/Events/downloads/euc2013/5-4-2_CST_EUC.pdf

[30] Electromagnetic Compatibility and Radio Spectrum Matters (ERM); Short-Range Devices (SRD); Ultra-Low Power Active Medical Implants (ULP-AMI) and Peripherals (ULP-AMI-P) Operating in the Frequency Range 402 MHz to 405 MHz; Part 1 and Part 2, European Telecommunications Standards Institute (ETSI) Std. EN 301 839-1/2 V1.3.1, 2007, [Online], Available: www.etsi.org

[31] F. Asgarian and A. M. Sodagar, "Wireless Telemetry for Implantable Biomedical Microsystems," Biomedical Engineering Trends in Electronics, Communications and Software, InTech, pp. 21-45, Jan. 2011.

ملخص البحث:

هنـــاك الكثيـــر مـــن التطبيقـــات الواعـــدة لشـــبكة المجســـات القابلـــة للزراعـــة فـــي جســـم الإنســـان. وتـــدعم المجسّـــات فـــي الشـــبكة وظـــائف مختلفـــة؛ مثـــل مراقبـــة الجلكـــوز وقيـــاس الإجهـــاد فـــي العظـــام. وتعمـــل هـــذه المجســـات بوجـــود رافعـــة مركزيـــة متصـــلة بمســـتقبل خـــارج الجســـم. والجدير بالذكر أن وجود رابط اتصال موثوق بين هذه المجسات أمر أساسي.

فـــي هـــذه الورقـــة، تـــم تقـــدير فقـــد المســـار بـــين هوائيـــاتٍ حَلقيـــة بيضـــوية ودائريـــة فـــي العضـــلات وعظمـــين مختلفـــين همـــا: عظـــم العَضُـــد وعظـــم الفخـــذ، عنـــد تـــردد مقـــداره 403 ميجـــاهيرتز. واتضـــح أن فقـــد المســـار بـــين العضـــلات وعظـــم العَضُـــد أكبـــر بمقـــدار 33 ديســـيبل مـــن فقـــد المســـار بـــين العضـــلات وعظـــم الفخـــذ. وعليـــه، يمكـــن بنـــاء رابـــطٍ معيـــاري يعمـــل بتعـــديلٍ قـــائم علـــى ترميـــز إزاحـــة الطـــور (PSK) بصـــورة مثاليـــة، فقـــط مـــن عظـــم الفخـــذ إلـــى العضـــلة الواقعة فوق الوِرك.

وتشـــكل النتـــائج التـــي تـــم الحصـــول عليهـــا فـــي هـــذا البحـــث مصـــدراً جيـــداً للبيانـــات لحســـابات ميزانيات الروابط في تطبيقات زراعة العظم.